Science of the Total Environment 888 (2023) 164141

Contents lists available at ScienceDirect

Science of the Total Environment

journal homepage: www.elsevier.com/locate/scitotenv

Dissolved black carbon as a potential driver of surface water heating dynamics in wildfire-impacted regions: A case study from Pyramid Lake, NV, USA

Brittany R. Kruger [a,*], Mark B. Hausner [b], Nathan Chellman [b], Morgan Weaver [a], Vera Samburova [c], Andrey Khlystov [c]

[a] Desert Research Institute, Division of Hydrologic Sciences, 755 E Flamingo Rd, Las Vegas, NV 89119, USA
[b] Desert Research Institute, Division of Hydrologic Sciences, 2215 Raggio Pkwy, Reno, NV 89512, USA
[c] Desert Research Institute, Division of Atmospheric Sciences, 2215 Raggio Pkwy, Reno, NV 89512, USA

HIGHLIGHTS

- High levels of dissolved black carbon were detected in a wildfire-impacted lake.
- Dissolved black carbon correlated to optically active organics in the lake.
- Dissolved black carbon caused accelerated water heating in lab experiments.
- Wildfire-derived dissolved black carbon may impact surface water heating dynamics.

GRAPHICAL ABSTRACT

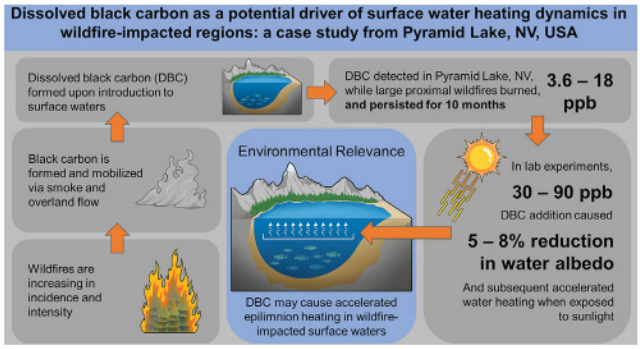

ARTICLE INFO

Editor: Pavlos Kassomenos

Keywords:
Black carbon
Dissolved black carbon
Water heating dynamics
Wildfire impacts

ABSTRACT

Black carbon (BC), pyrogenic residues resulting from the incomplete combustion of organics, are liberated from wildfires at high rates. Subsequent introduction to aqueous environments via atmospheric deposition or overland flow results in the formation of a dissolved fraction, called dissolved black carbon (DBC). As wildfire frequency and intensity increases along with a changing climate, it becomes imperative to understand the impact a concurrent increase in DBC load might have to aquatic ecosystems. In the atmosphere BC stimulates warming by absorbing solar radiation, and similar processes may occur with surface waters that contain DBC. In this work we investigated whether the addition of environmentally relevant levels of DBC could impact surface water heating dynamics in experimental settings. DBC was quantified at multiple locations and depths in Pyramid Lake (NV, USA) during peak fire season while two large, proximal wildfires burned. DBC was detected in Pyramid Lake water at all sampled locations at concentrations (3.6–18 ppb) significantly higher than those reported for other large inland lakes. DBC was positively correlated (R^2 = 0.84) with chromophoric dissolved organic matter (CDOM) but not bulk dissolved or total organic carbon (DOC, TOC), suggesting that DBC is a significant component of the optically active organics in the lake. Subsequent lab-based experiments were conducted by adding environmentally relevant levels of DBC standards to pure water, exposing the system to solar spectrum radiation, and creating a numerical model of heat transfer based on observed temperatures. The addition of DBC at environmentally relevant orders of magnitude caused reductions to shortwave albedo when exposed to the solar spectrum, which resulted in 5–8 % more incident radiation being absorbed by water and changes to water heating dynamics. In environmental settings, this increase in energy absorption could translate to increased heating of the epilimnion in Pyramid Lake and other wildfire-impacted surface waters.

* Corresponding author.
E-mail address: brittany.kruger@dri.edu (B.R. Kruger).

http://dx.doi.org/10.1016/j.scitotenv.2023.164141
Received 5 December 2022; Received in revised form 21 April 2023; Accepted 9 May 2023
Available online 11 May 2023

1. Introduction

Black carbon particles (BC) are organic residues formed by fossil fuel and biomass burning, and have been shown to stimulate warming in the atmosphere due to their significant light absorption capacity and subsequent heating (Sengupta et al., 2018; Samburova et al., 2016; Stocker et al., 2013; Jacobson, 2001; Jacobson, 2002). While frequently studied in an atmospheric setting, BC has only recently been identified as a major component of aquatic carbon cycles, and its behavior and characteristics within those systems are not yet fully understood (Wagner et al., 2018). In aqueous systems, dissolved BC (DBC)—functionally defined as BC that passes through a designated filter pore size (Li et al., 2019; Qu et al., 2015)—forms as different BC constituents undergo partitioning, chemical transformation, and dissolution, and DBC has been shown to accumulate in surface waters as a result of atmospheric deposition and overland flow (Zigah et al., 2012; Burkhard et al., 2008). Continued fossil fuel burning combined with the predicted and observed increase in wildfire frequency and intensity accompanying a warming climate (Flannigan et al., 2000; Westerling and Bryant, 2008; Abatzoglou and Kolden, 2011; Iglesias et al., 2022; Wuebbles et al., 2017; Westerling et al., 2006) will likely result in increasing DBC concentrations in surface waters of fire-impacted regions in coming decades. Wildfires seasons are becoming longer in both the western United States and globally in association with climate-induced shifts toward aridity in many regions (Liu et al., 2010; Jolly et al., 2015). Longer fire seasons and increased aridity drive the increase in wildfire duration and severity observed in recent years (Iglesias et al., 2022; Jolly et al., 2015). Black carbon is liberated from these wildfires, and the long-range aerosol transport of wildfire-sourced BC is also well documented, with elevated atmospheric BC concentrations clearly tied to wildfire activity at distant locations (Ahlberg et al., 2023; Byčenkienė et al., 2014). That aerosolized black carbon has the potential to become dissolved black carbon as particles are deposited onto surface water bodies or watersheds (Wagner et al., 2018; Burkhard et al., 2008). Therefore, the observed increase in global wildfire activity and severity in multiple regions has the potential to impact surface water DBC levels on a global scale. Whether and how this potential elevated level of DBC might impart ecosystem-scale changes to aquatic systems is unknown.

The light absorption and heating behavior of BC in the atmosphere raises the question of whether DBC may impart similar absorption and heating properties to surface waters in which it accumulates. Similarly, BC deposition on snow has been shown to lower snow albedo and subsequently accelerate snowmelt as a function of increased radiation absorption (Flanner et al., 2007; Kaspari et al., 2015), and an analogous process may occur in surface waters. Because BC is generated across a spectrum of combustion temperatures and from a diversity of biomolecules (Baldock and Smernik, 2002; González-Pérez et al., 2004), the resulting DBC fraction can contain a continuum of non-aromatic, saccharide-like molecules to polycondensed aromatic molecules (Wagner et al., 2018). The relative proportion of these molecules within the DBC fraction is then further susceptible to photoalteration (Li et al., 2019; Fu et al., 2016), bioalteration (Baldock and Smernik, 2002; Hamer et al., 2004), and aggregation/precipitation (Xu et al., 2017) events specific to the aquatic environment in which it resides, all of which could affect light absorption and subsequent heating dynamics.

While DBC is present in small amounts relative to bulk total or dissolved organic carbon (TOC, DOC) in most aquatic habitats (Wagner et al., 2018), the strong light-absorptive properties of common DBC moieties could result in a disproportionate impact to water heating dynamics. In aqueous settings, dissolved organic matter is well known to absorb light across the UV to infrared spectrum, with the most optical activity centered around mid-range UV (~254 nm) absorption by aromatics (Weishaar et al., 2003). While spectroscopic and elemental analysis has shown that DBC is generally less aromatic that its parent biomass-derived BC material (Qu et al., 2015), the aromaticity of DBC is generally higher than that of other dissolved organics in aqueous systems (Wagner et al., 2018), suggesting that its contribution to absorption-driven heating could be significant. The way this DBC-driven heating may affect overall water quality and lake ecology is unknown and is a driving motivation for this work.

In this study we sought to investigate how the presence of DBC might affect the heating dynamics of surface water. To do so, we quantified DBC at various surface and deep-water locations in Pyramid Lake (NV, USA, Fig. 1) during peak fire season in 2021 while two large, proximal wildfires (Caldor and Dixie) burned. We then conducted lab-based experiments and created a numerical model of heat transfer for each experiment to optimize values of surface albedo and attenuation rate based on observed temperatures to determine whether environmentally relevant concentrations of DBC affected water heating rates and dynamics, and whether photoalteration of DBC was observable as a result of experimentation.

2. Methods

2.1. Field study site and wildfire conditions

Environmental water samples were collected for DBC quantification from Pyramid Lake, Nevada (Fig. 1) on August 31 and September 1, 2021. Pyramid Lake is a large monomictic endorheic basin (487 km^2 surface area, 29 km^3 volume (Galat et al., 1981)) managed in totality by the Pyramid Lake Paiute Tribe (PLPT). It is home to two federally listed fish species, Lahontan cutthroat trout (LCT) and the endemic Cui-ui sucker, which are critical to the economic and cultural wellbeing of the PLPT. The PLPT manage successful and productive fisheries operations in the lake and altered ecosystem dynamics within the lake could negatively impact those operations.

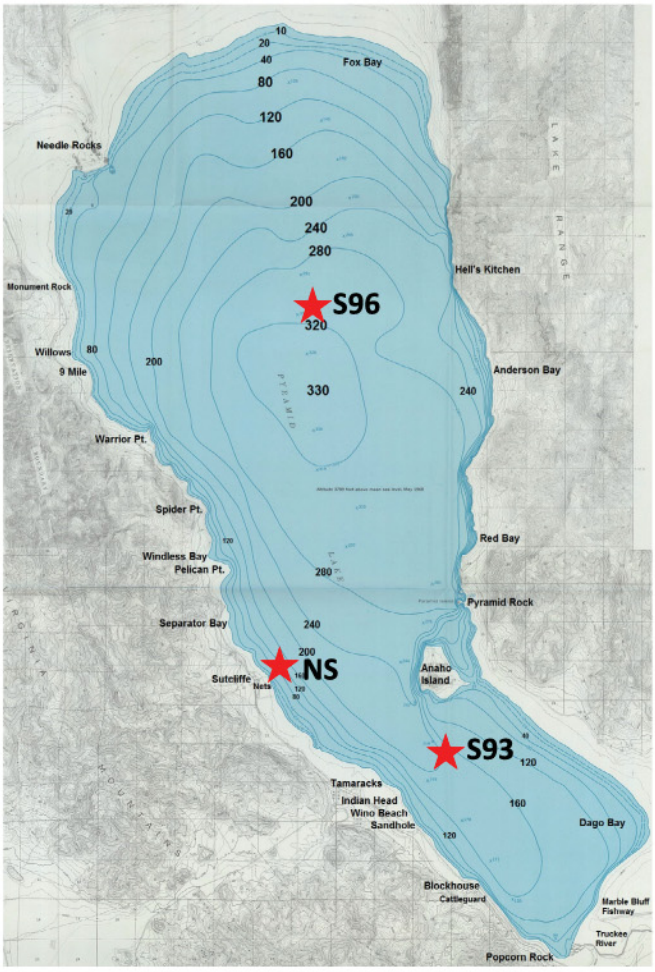

Fig. 1. Water sampling locations within Pyramid Lake, NV, USA. Map modified from Harris, 1970 (Harris, 1970) (depth contours labeled in ft).

During the August/September 2021 water sampling, Pyramid Lake and the surrounding region had for weeks been heavily impacted by smoke from two large, proximal wildfires (Fig. 2). The Dixie Fire, burning ~72 km west/northwest from Pyramid Lake, was 3267 km^2 in size and 45 % contained at the time of sampling, and had been burning for 1.5 months (*Dixie Fire Incident Report*, n.d.). The Dixie Fire is currently the second largest fire in California history (*Dixie Fire Incident Report*, n.d.). The Caldor Fire, burning ~126 km southwest from Pyramid Lake, was 773 km^2 in size and 16 % contained at the time of sampling, and had been burning for two weeks (*Caldor Post-Fire BAER Information - InciWeb the Incident Information System*, n.d.). The week prior to water sampling, the Air Quality Index (AQI) for fine particle pollution ($PM_{2.5}$) in the Pyramid Lake basin was frequently at "Unhealthy for Sensitive Groups" (AQI = 101–150) and "Unhealthy" (AQI = 151–200) levels. During water sampling, smoke plumes from the Dixie Fire were clearly visible and, depending on wind direction, would funnel across the north end of the lake (Fig. 2A, B) or would engulf the entire lake basin. Ash was observed by eye to be falling from smoke plumes onto the lake surface (Fig. 2B), and large ash particulates were subsequently observed floating on the lake surface during water sampling at both mid-lake (Fig. 2C) and near-shore locations.

2.2. Pyramid Lake sample collection and analysis

Water sampling was conducted at three locations in Pyramid Lake (Fig. 1), and at three depths, in coordination with the Pyramid Lake Fisheries Department. Three water depths (surface (0 m), 5 m, 80 m) were sampled at open lake location S96, with lake profiling conducted at this site via SBE 19plus SeaCAT CTD profiler (Sea-Bird Scientific, Bellevue, WA, USA) at 1 m intervals. Additional surface water (0 m) was sampled at open lake location S93 and nearshore location NS. At S96, bulk water samples were collected aboard the Pyramid Lake Tribal Fisheries boat by multiple 3.5 L Van Dorn casts to the target depth, and subsequent collection into acid washed glass and polytetrafluoroethylene (PTFE) carboys. Van Dorn sampling is a standard method for collecting water column samples when low vertical resolution is needed, and has been utilized for decades to obtain vertical records of water quality, chemical, and biological parameters in lakes (Van Dorn, 1956; Tran et al., 2021; Hudson et al., 1999). At S93 and NS surface water was collected by direct immersion of acid washed glassware. Water samples were transported to the Pyramid Lake Fisheries Adeline Davis Research Laboratory (Sutcliffe, NV) and processed within 6 h of collection.

Bulk water was subsampled and filtered (via combusted (450 °C for 4.5 h) quartz fiber filters in acid washed filter housings), then preserved as needed for geochemical analysis of 5 m and 80 m water from S96 (performed by ACZ Labs, Inc., Steamboat Springs, CO), and TOC and DOC. Water samples for TOC/DOC were subsampled into acid washed and combusted (10 % HCl for 4 h, followed by deionized water (DI) rinsing, followed by combustion at 450 °C for 4.5 h) amber glass vials, acidified to pH = 2 with 12 N HCl, and kept at 4 °C until analysis (performed by Anatek Labs, Moscow, ID, USA). Unfiltered water subsamples were collected into acid washed and combusted (see above) amber glass vials and stored at 4 °C for Single Particle Soot Photometer (SP2; Droplet Measurement Technologies, Boulder, CO, USA) analysis of black carbon within 48 h of collection. The SP2 method has been used extensively to measure black carbon in ice, snow, rainwater, atmospheric, and lake samples (McConnell et al., 2021; Gleason et al., 2022; Mori et al., 2014; Chellman et al., 2018; Arienzo et al., 2019; Bisiaux et al., 2011).

Water samples were introduced to the SP2 analytical system using an autosampler and peristaltic pump, filtered inline using a 20 um stainless steel filter to remove any large particles that could potentially clog flowlines, and aerosolized using an Apex-Q nebulizer (Elemental Scientific, Omaha, NE). The dry aerosol generated by the nebulizer was passed to the SP2 for BC determination by laser-induced incandescence (Stephens et al., 2003). The SP2 is sensitive to submicron diameter, highly refractory soot particles referred to as refractory BC (rBC) (Torres et al., 2014; Petzold et al., 2013). Since the SP2 rBC measurement range is limited to rBC particles with diameters <400 nm, we consider rBC and DBC synonymous for the purposes of this study. The instrument used in this study was internally calibrated using the BC-like material Aquadag to measure rBC particles up

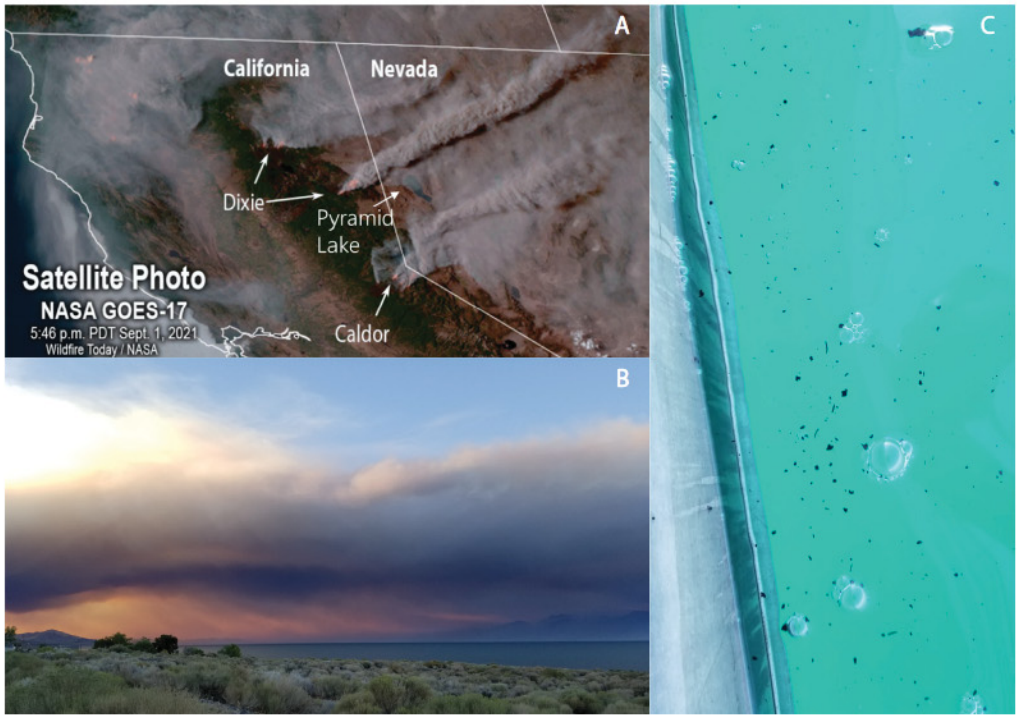

Fig. 2. NASA satellite imagery showing Dixie and Caldor Fire locations on Sept 1, 2021 relative to Pyramid Lake (A), a photo taken Sept 2, 2021, from the western edge of Pyramid Lake, looking north, showing the Dixie Fire smoke plume and associated falling ash (B), large ash particulates floating on the surface of the lake at open water sampling location S96 on Aug 31, 2021 (C).

to ~400 nm in diameter, thus we consider rBC as measured by the SP2 to be synonymous with the operational definition of DBC as BC particles passing through a 0.5 μm filter. Aqueous standards were run immediately prior to sample analysis as an external calibration to account for changes in the sample introduction system or nebulization efficiency. The average detection limit for the SP2 measurements was 0.40 ± 0.23 ppb (1σ; n = 10 analysis days) and the average percent error for quality control standards ranging from 1 to 30 ppb was 13 ± 12 % (1σ; n = 11). Additional water samples for only SP2 quantification of DBC were collected from the same sample locations in July 2022 by direct filling of acid washed and combusted (see above) vials from the Van Dorn sampler.

2.3. Water heating experiments

Because no information is currently available about how DBC affects water heating dynamics, we conducted lab experiments to generate baseline data on this topic with DBC as an isolated variable. Two heating experiment trials (HE_40ppb and HE_40ppb_dup) were conducted indoors using heat lamps as the light source, and three trials (HE_30ppb, HE_30ppb_dup, HE_90ppb) were conducted outdoors using sunlight as the light source (Table 1). For indoor trails, two 22 L glass aquarium tanks (21.5 cm wide, 41 cm long, 26 cm high) were utilized concurrently, one a control (no DBC addition) and one with DBC added. Which tank received control vs. experimental treatments was randomized between trails. Aquarium thermometers (VIVOSUN LCD Digital, accurate to +/− 1 °C, Ontario, CA, USA) were affixed to the internal sides of each tank at 2.5 cm from the tank bottom and 4 cm from the tank top. Per trial, 17 L of milli-Q (MQ) water (stored in acid washed PTFE carboys overnight in a 10 °C incubator) was added to each tank, along with either room temperature MQ (control) or room temperature DBC master solution (experiment) to achieve the experimental concentrations listed in Table 1. Outdoor trials were conducted using the same tank assembly and filling parameters described above, but were all run concurrently, with three tanks serving as DBC addition treatments and one serving as control. After filling, the top thermometer was submerged by 1.25 cm. DBC master solution was made by adding fullerene soot powder (C_{60} and C_{70}, Sigma-Aldrich 572,497, St. Louis, MO, USA) to MQ water (at a ratio of 1 g soot into 500 mL MQ) in an acid washed/combusted 1 L bottle. The bottle was capped and inverted 10×, sonicated for 30 min with 10× inversions every 5 min, and passed through combusted 0.3 μm nominal pore size glass fiber membrane filters (Sterlitech GF-75, Auburn, WA, USA) via acid washed/combusted glass filtration apparatus. Resulting <0.3 μm filtrate was used as the DBC master solution. Commercially available fullerene soot was chosen as the parent material for these first heating experiments to allow for confident repeatability of experimental conditions between trails.

Once tanks were filled, an insulative foam barrier was added around the openings and sides of the tanks, ensuring that heat entered the treatments primarily from the top (water surface) rather than the tank sides. The control and experimental treatment tanks were then concurrently subjected to heating conditions as described in Table 1, using either heat lamps or sunlight as the heat source. When heat lamps were used, two were used concurrently (Wuhostam 75 watt 780–1400 nm Ceramic Infrared Heat Lamp and Repti Zoo 100 watt (W) 270–800 nm Full Spectrum Sun Lamp) to apply both visible and infrared wavelengths via dual bulb light fixture situated 1 m above the tanks. Carbon contamination during the experiment was ruled out by quantifying DBC at experiment initiation and completion in both experimental and control trials, with no significant differences found.

Table 1
Initial experimental (exp) and control (ctl) conditions for water heating experiments (HE) conducted at various DBC concentrations.

Treatment	Exp [DBC], ppb (st dev)	Ctl [DBC], ppb (st dev)	Experiment light source	Trial duration, minutes
HE_40ppb	45 (1.0)	0.1 (0.1)	Heat-lamps	120
HE_40ppb_duplicate	40 (1.2)	0.2 (0.2)	Heat-lamps	120
HE_30ppb	34 (0.8)	0.2 (0.2)	Sunlight	180
HE_30ppb_duplicate	35 (0.7)	0.2 (0.2)	Sunlight	180
HE_90ppb	91 (1.3)	0.2 (0.2)	Sunlight	180

2.4. Heat transfer modeling

To develop a preliminary quantitative description of how DBC affects heating dynamics in a water column, we created a numerical model of heat transfer for each experiment to optimize values of surface albedo and attenuation rate based on observed temperatures. The model is a simplified version of the heat transfer model described by Hausner et al. (2013) (Hausner et al., 2013), and considers exponential attenuation of downwelling radiation according to the Beer-Lambert Law, reflection of radiation at the bottom of the tank and exponential attenuation of upwelling (reflected) radiation absorbed as heat, and conductive heat transfer within the water column. The model domain included only the 24 cm deep water column, with the upper boundary simulated as a radiative flux boundary. Side boundaries were assumed to be zero-flow boundaries to simulate the insulation placed around the tanks. The bottom boundary was simulated as a semi-reflective interface, allowing a fraction of the solar irradiance reaching the boundary to be reflected upwards and pass through the water column a second time. In the laboratory models, the solar irradiance not reflected at the bottom boundary was assumed to leave the system; in the outdoor models the unreflected irradiance was assumed to be absorbed as heat at the bottom of the water column.

The radiation at a given depth in the tank was simulated according to Eq. (1)

$$I(z) = I_0(1 - A)\exp(-\alpha z) \tag{1}$$

where $I(z)$ is the radiation at depth z, I_0 is the vertical component of total radiation incident on the water surface, A is the surface albedo, and α is the attenuation rate within the water column. The energy absorbed as heat by any given control volume is calculated as $\frac{dI}{dz}$, or the difference between downwelling radiation at the top of the control volume and downwelling radiation at the bottom of the control volume.

A fraction of the radiation that reached the bottom of the tank was reflected and attenuated as it passed upwards through the water column. The radiation that was not reflected was assumed to be removed from the system. Upwelling radiation is given by Eq. (2)

$$I'(z) = I_0(1 - A)\exp(-\alpha z_{max})A\exp(-\alpha z') \tag{2}$$

where I′(z) is the upwelling radiation at depth z, z_{max} is the maximum depth of the tank, and $z' = (z_{max} - z)$ is the distance from the bottom of the tank to depth z. Upwelling radiation absorbed as heat is given by $\frac{dI'}{dz}$, in a calculation similar to the one above for downwelling radiation.

Conductive heat flux within the water column was simulated using Eq. (3)

$$q_c = -\lambda\frac{dT}{dz} \tag{3}$$

where q_c is the conductive heat flux (W m^{-2}), λ is the thermal conductivity of water, and $\frac{dT}{dz}$ is the vertical thermal gradient within the water column.

Eqs. (1)–(3) return vertical energy fluxes (W m^{-2}) in the water column. The model sums these fluxes for each discrete control volume according to Eq. (4) and converted the change in stored energy to a change in temperature using Eq. (5). In Eq. (4), z_{top} and z_{bottom} indicate the depth of water at the top and bottom of the control volume, respectively.

$$\frac{dE_i}{dt} = \left[I(z_{top}) - I(z_{bottom})\right] + \left[I'(z_{bottom}) - i'(z_{top})\right] + q_c(z_{top}) + q_c(z_{bottom}) \tag{4}$$

$$\frac{dT}{dt} = C_v V_i \frac{dE}{dt} \tag{5}$$

in which $\frac{dT}{dt}$ is the change in temperature with respect to time, C_v is the volumetric capacity of water (assumed to be constant at 4.18×10^6 J m^{-3} K^{-1}), and V_i is the volume of the discrete depth unit i.

The model of heat transfer in the outdoor experiments differed from the laboratory model only in the handling of radiation at the bottom of the tank. In the laboratory model, radiation that was not reflected was assumed to leave the system. In the outdoor model, the radiation that was not reflected upward was added to the bottom cell as heat to reflect the layer of black plastic underneath the tank in this set of experiments.

In both models, the temperature-dependent effects of density on volumetric heat capacity are neglected. No evaporation or sensible heat fluxes were simulated at the water surface, and the one-dimensional model assumes no heat transfer through the walls of the tank. The model was programmed as an ordinary differential equation (ODE) in MATLAB and simulated using ode15, a MATLAB ODE solver. The model was discretized into 24, 1-cm control volumes, and temperatures were simulated at the center of each node. Temporal discretization is determined by the MATLAB ODE solver based on the simulated gradients and numerical stability thresholds. Simulated water temperatures were compared to water temperatures observed at the two aquarium thermometers, and the root mean square error (RMSE) of the simulation was used as the metric of model error. Values of the surface albedo (given the assumed incident radiation) and attenuation rate were optimized using the MATLAB function fminsearch to minimize the RMSE. Optimization was repeated with multiple initial values, representing the range of expected values for albedo (0.01–0.99) and attenuation rate (10^{-2}–10^3 m^{-1}). MATLAB scripts for the heat transfer model and the optimization functions are available on Dryad.

The laboratory experiments involved two lamps and focused on a combination of visible and infrared light. Visible light was provided by a 100 W 270–800 nm full spectrum sun lamp, for which expected attenuation rates are on the order of 10^{-2} to 10^0 m^{-1}. Infrared radiation was provided by a 75 W 780–1400 nm ceramic heat lamp, for which expected attenuation rates are on the order of 10^0 to 10^3 m^{-1}. The visible light lamp was assumed to have half its radiation falling on the water surface, while the infrared lamp was assumed to fall totally on the water surface, for a total irradiance of 1414 W m^{-2} ($\frac{50\ W + 75\ W}{0.0884\ m^2}$).

In the outdoor experiments, the tanks were exposed to the full solar spectrum, which is largely contained between 250 nm and 25 μm in wavelength. The expected attenuation rates for this range of frequency vary from 10^{-5} to 10^6 m^{-1}, but the peak of the solar spectrum falls into the visible light band, with attenuation rates on the very low end of that range. Total shortwave radiation between 1035 h and 1345 h PDT in late April averages approximately 900 W m^{-2} (based on the National Renewable Energy Laboratory (*NPCS Solar Calendars*, n.d.)). In addition to solar radiation, the tanks were exposed to longwave atmospheric radiation (i.e., infrared). Air temperature during the experiments ranged from 81 to 85 °F (27–29 °C) and vapor pressure was approximately 6 mb based on United States National Weather Service records for the Harry Reid International Airport (2.4 km from the experiment site). Given atmospheric emissivity at that temperature and humidity (Staley and Jurica, 1972), this longwave radiation would have been approximately 440 W m^{-2}. Total irradiance in the outdoor experiments was therefore assumed to be 1340 W m^{-2}.

With the values of incident radiation noted above, the models were optimized to minimize the root mean square error between the observed and simulated temperatures at the top and bottom of the tanks. The optimization routine allowed the surface albedo and attenuation rates to vary. Each experiment was optimized individually.

2.5. Dissolved carbon analysis

The nature of DOM from Pyramid Lake and the DBC from experimental trials (at both experiment initiation and conclusion) was assessed via UV–Vis range scanning spectrophotometry (Genesys 150) with absorbance measured from 800 to 200 nm at 1-nm increments. Resulting absorbance data was backscatter corrected and transformed into absorption coefficients according to Eq. (6):

$$a = \frac{2.303A}{l} \tag{6}$$

where a = absorption coefficient (m^{-1}), A = absorbance, and l = path length (m) (Helms et al., 2008). Using absorption coefficient data, the E2/E3 ratio was calculated (ratio of a at 250 to 365 nm) as an indicator of relative molecule size (De Haan and De Boer, 1987), specific UV absorbance (SUVA254) was calculated (a at 254 nm normalized to dissolved organic carbon concentration) as an indicator of aromaticity (Weishaar et al., 2003), and total chromophoric dissolved organic matter (CDOM) was quantified by integrating a from 250 to 450 nm.

3. Results and discussion

3.1. DBC in Pyramid Lake

At the time of water sampling in 2021 Pyramid Lake was strongly stratified with the thermocline transition zone constrained between ~15–30 m depth, placing sampling depths for this work clearly within epilimnion (0 m and 5 m) and hypolimnion (80 m) zones (Fig. 3). DBC was detectable at all locations and depths sampled in Pyramid Lake, and DBC was still detectable at all locations when re-sampled 10 months later (Table 2). During initial water sampling, at S96, DBC concentrations were found to be highest at the surface (4.54 ppb, standard deviation (stdev) = 1.16 ppb) with lower concentrations found at 5 m and 80 m (3.72 (stdev = 1.01) and 3.58 (stdev = 1.84) ppb, respectively). Higher DBC concentrations were found in surface water (0 m) at the open water location S93 (7.58 (stdev = 3.63) ppb) and at the nearshore water sampling location NS (18.1 (st dev = 6.2) ppb). These concentrations are 1–2 orders of magnitude greater than DBC measured via the same SP2 quantification method in 2007 at a mid-lake open water location of Lake Tahoe (~0.3 ppb, Lake Tahoe is located 100 km SW of Pyramid Lake and is a source to Pyramid Lake via the Truckee River), during a seasonal pulse of BC attributed to a proximal wildfire (Bisiaux et al., 2011). Similar levels of DBC were detected upon

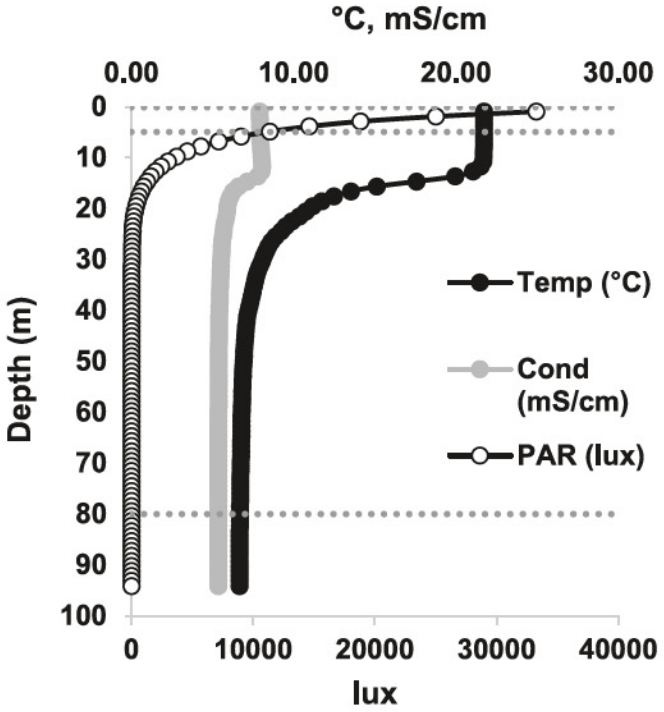

Fig. 3. CTD profile at Pyramid Lake station S96 during 2021 sampling event. 0 m, 5 m, 80 m water sampling depths marked by dotted lines.

Table 2
Carbon fraction concentrations and characteristics for Pyramid Lake environmental water samples (S96, S93, NS) measured at various water depths (0, 5, or 80 m). All water samples were collected in September 2021 unless otherwise noted. DBC:TOC ratio calculated using the Sept 2021 DBC values.

	[DBC], ppb (st dev),	[DBC], ppb (st dev), July 2022	[TOC], ppm (avg error)	[DOC], ppm (avg error)	DBC: TOC (%)	E2/E3	CDOM	SUVA254
S96_0m	4.5 (1.2)	8.6 (3.3)	16.4	–	0.027	11.9	633	–
S96_5m	3.7 (1.0)	5.3 (2.3)	12.3 (0.2)	11.9 (0.3)	0.030	16.8	535	1.10
S96_80m	3.6 (1.8)	14.2 (3.7)	11.2 (0)	11.3 (0.1)	0.032	29.9	425	1.05
S93_0m	7.6 (3.6)	5.0 (2.3)	13.2	–	0.058	20.6	510	–
NS_0m	18 (6.2)	4.0 (2.1)	12.2 (0)	11.7 (0.1)	0.15	7.8	1000	1.55

water re-sampling in July 2022, though with concentrations appearing to shift to different lake locations and depths. This suggests that DBC may persist in the lake over time, and that DBC distribution in the lake may be tied to water circulation dynamics.

In other large lake systems BC quantification has typically focused on the suspended particulate fraction (≥ 0.7 μm) rather than DBC, with 2–5 ppb particulate BC found in an isothermal water column of Lake Superior (Zigah et al., 2012), and 0.2–0.5 ppb found in the epilimnion of a stratified water column in Lake Michigan (while hypolimnion values were ≤ 0.2 ppb) (Burkhard et al., 2008). Thus, many DBC concentrations measured in Pyramid Lake in this work were greater even than levels of particulate BC reported for other lakes and could represent significant input from the proximal wildfires burning during initial water sampling. Further, the SP2 method used here efficiently captures signal from highly refractory (elemental) BC components, but not BC at lower thermochemical classifications. Even within the refractory BC pool, an underestimation of ~34 % by mass has been shown via SP2 in rainwater samples (Torres et al., 2014). These two points suggest that the true levels of DBC at all Pyramid Lake water sampling locations may be higher than reported.

Given the increasing frequency and intensity of wildfires in the region (Westerling and Bryant, 2008; Iglesias et al., 2022; Wuebbles et al., 2017), the high (and possibly higher than reported) DBC levels seen in Pyramid Lake and the persistence of DBC in the water column for at least 10 months could suggest a tendency for DBC to accumulate over time in surface waters and should be further investigated. This possibility is supported by research that has suggested that less BC mineralization and oxidation occurs in conditions of complete water saturation, when compared to unsaturated or alternating saturated-unsaturated conditions (Nguyen and Lehmann, 2009). That BC degradation is inhibited by continuous saturation may support the detection of aged BC (5000–13,900 ^{14}C years) found in saturated environments (riverine particulates (Masiello and Druffel, 2001) and marine sediments (Masiello and Druffel, 1998)), while BC in aerated top soils has been found to be decades to centuries old (Bird et al., 1999). Additionally, photoexposed DBC has been shown to have enhanced colloidal stability, making it resistant to aggregation and subsequent sedimentation which could contribute to its accumulation over time (Xu et al., 2017).

Spectral analysis of the bulk DOM in Pyramid Lake (Table 2) across the UV–Vis spectrum showed nearshore surface water DOM to be notably more aromatic (SUVA 254 = 1.55) and higher in chromophoric dissolved organic matter (CDOM = 1000), and to have the largest particle size (E2/E3 = 7.8) relative to other Pyramid Lake water samples (SUVA254 = 1.05–1.1, E2/E3 = 11.9–29.9, CDOM = 425–633). At open lake location S96, particle size, CDOM, and aromaticity decreased with depth. With all Pyramid Lake water samples considered, DBC was an extremely small component of the TOC in the lake (0.03–0.2 wt%), and yet DBC content was positively correlated to CDOM content ($R^2 = 0.84$) but not DOC ($R^2 = 0.04$) or TOC ($R^2 = 0.03$) content. This suggests differential controls on the distribution of DBC vs. bulk DOC/TOC within the lake, and that DBC is a significant component of the light-absorbing DOM within the Pyramid Lake.

The differential distribution of DBC concentrations, and therefore CDOM, may be tied to the thermochemical status of the DBC. The higher DBC concentrations seen in all three surface water samples relative to 5 m and 80 m samples suggests deposition directly to the epilimnion as a primary route of DBC addition to the lake, and potentially preferential accumulation in the epilimnion. The much higher DBC seen in the nearshore water sample (18.06 ppb) relative to the open lake samples (3.23–7.58 ppb) could suggest that an unidentified nearshore input of DBC exists, or that DBC preferentially collects at nearshore locations as a function of water circulation patterns in the lake upon formation. The more hydrophobic nature of DBC (relative to DOC or TOC) makes the latter explanation more likely, as it makes DBC more susceptible to redistribution.

3.2. Water heating experiments

The addition of DBC at environmentally relevant concentrations affected water heating dynamics in all experimental trials, with variable results seen between light source (heat-lamp vs. sunlight) trails (Fig. 4). When heat-lamps were applied as the heat source, water at 1.5 cm below the surface with 40 ppb DBC added heated more quickly and stayed warmer than the control (0 ppb DBC), while no difference in heating rate was observed at 22.5 cm water depth (Fig. 4A). When sunlight was applied as the heat source, water at 1.5 cm below surface heated at similar rates despite DBC concentration (0 ppb (control), 30 ppb, 90 ppb), while water at 22.5 cm below surface heated more quickly and remained warmer (relative to the control) when DBC was present at either 30 ppb or 90 ppb (Fig. 4B). These differences give important insights into the potential impact DBC might have on environmental surface water heating.

Heat transfer modeling of these results produced simulated vs. observed temperatures shown in Fig. 5A and B, respectively. The Nash Sutcliffe Efficiencies (Nash and Sutcliffe, 1970) of the laboratory and outdoor models are 0.984 and 0.885, respectively. Nash Sutcliffe Efficiency is a measure of model accuracy; a value of zero indicates that the model is functionally equivalent to using the mean temperature, while a value of one indicates a perfect model.

In each model, the temperatures in the bottom of the tank are generally simulated more accurately than those at the top of the tank. This reflects the assumption of a single attenuation rate for a range of incident wavelengths. This assumption, which operates in both models, is at odds with the fact that the incident radiation in both experiments is a combination of shortwave (i.e., visible light) and infrared. The typical attenuation rates for visible light in water are several orders of magnitude less than the attenuation rates for infrared radiation. In both experiments, there are additional surface heat fluxes – sensible heat flux and latent heat flux – that act on the water surface but are not included in the model, and these fluxes are much greater in the outdoor experiments than in the laboratory. In both sets of experiments the lower temperatures are simulated more accurately than the upper temperatures, but this difference is exaggerated in the outdoor experiments. This exaggeration, seen in the shape of the scatter plot in Fig. 5B, is due to the effects of the neglected surface flux. While the bottom temperatures are accurately predicted, the surface temperatures exhibit the curve seen in the figure; this systematic error is likely driven by the omission of latent heat flux due to evaporation, which cools the water. Latent heat flux increases with increasing temperature, leading the model to overpredict surface temperatures late in the experiment. The early-time underprediction of surface temperatures is an artifact of the optimization routine, which attempts to minimize the total error through the course of the experiment. Despite these shortcomings, both models generally predict the pattern of the water temperatures.

In the laboratory experiments, the addition of DBC had minimal effect on the surface albedo (Table 3), but increased the attenuation rate in both

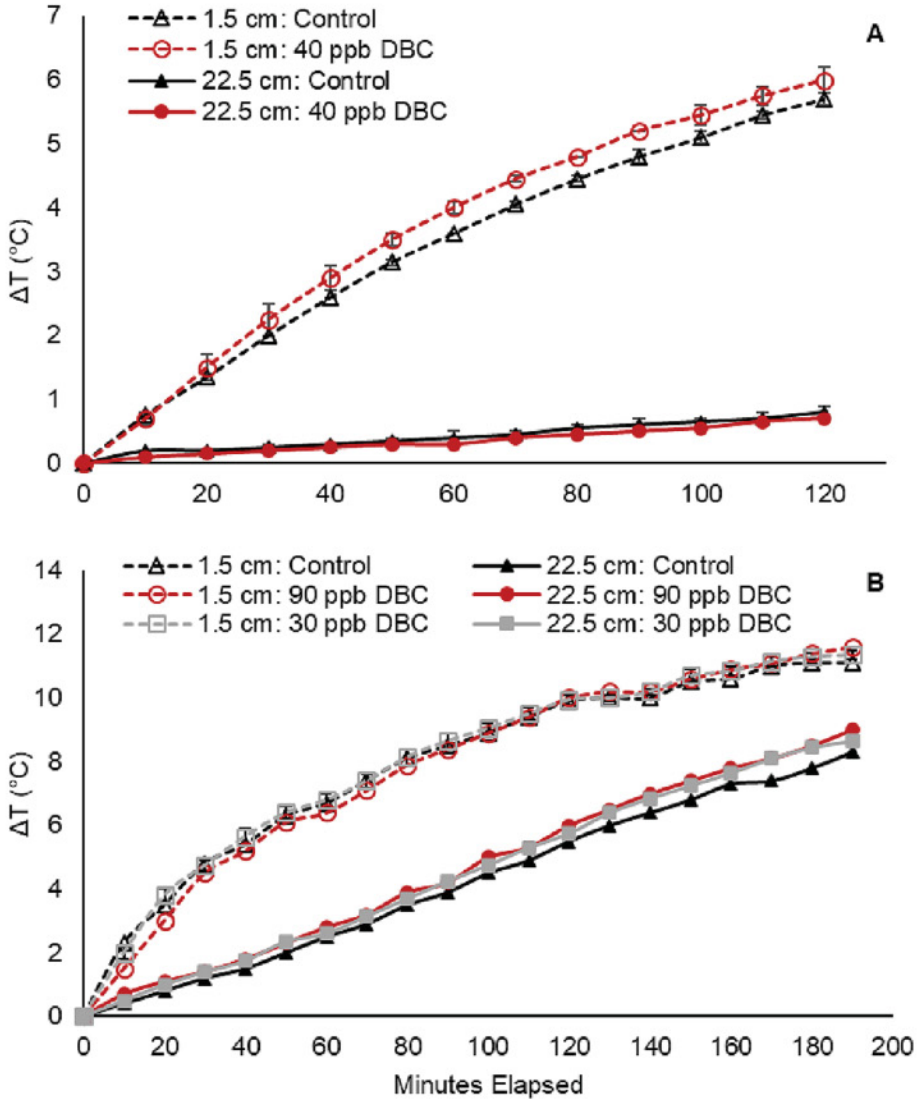

Fig. 4. Water heating observed during trials conducted with heat-lamps (A) or sunlight (B) as the heating source and at multiple DBC concentrations, displayed as the change in temperature (ΔT (°C)) relative to initial temperature. Error bars are shown for concentrations with replicates (all except sunlight control and sunlight 90 ppb) though are often smaller than the data markers.

HE_40ppb and HE_40ppb_dup. This resulted in the experimental tanks having higher temperatures than the controls at the tops of the tanks and minimal differences at the bottoms. The laboratory experiments are dominated by infrared radiation, which is generally absorbed efficiently by water. Water containing DBC has increased attenuation rates for infrared radiation – it will absorb infrared radiation more readily. This leads to higher temperatures near the water surface, and minimal temperature changes lower in the tank. The relatively constant albedo, however, indicates that water with DBC does not absorb more infrared radiation than clean water; the heat absorbed is simply distributed differently.

The outdoor experiments were driven by the full solar spectrum, including UV (approximately 8 %), shortwave (visible light; approximately 42 %) and infrared radiation (approximately 50 %), with a much wider range of infrared than the laboratory experiments. The order-of-magnitude reduction in the optimized attenuation rates from the outdoor experiments is consistent with the reduction in the fraction of IR radiation – visible light and UV radiation are able to penetrate much farther into the water column than IR radiation does. The optimized albedos in the outdoor experiments were significantly reduced from those found in the laboratory experiments, and the outdoor experimental treatments had albedos 5–8 % lower than the control treatment. The change in the nature of the incident radiation between the experiments suggests that this decrease in albedo is largely associated with visible light rather than with IR.

The observed difference in longwave attenuation rate is consistent throughout the laboratory experiments but does not have significant ecological implications. Longwave radiation is quickly absorbed in the water column; if it attenuates slightly faster in water with DBC, that faster attenuation is negligible compared to the changes in the propagation of shortwave radiation in the water column.

In contrast to the longwave attenuation rate, the reduction in shortwave albedo associated with DBC in the outdoor experiments has significant implications for the Pyramid Lake ecosystem. The experimental treatments containing DBC absorbed 5–8 % more of the incident radiation than the control treatment did. In a deep lake with an aphotic zone, all of that additional energy will be translated to heat in the water column. Absorption of additional radiation as heat will result in elevated water temperatures associated with DBC in the water column. The distribution of this additional heat will depend on the attenuation rates and lake mixing dynamics, but these results indicate that increases in the DBC content of the lake may lead to an increase in heat entering the lake.

Because these experiments were designed and performed to understand the influence of DBC in isolation, the quantitative results reported here are

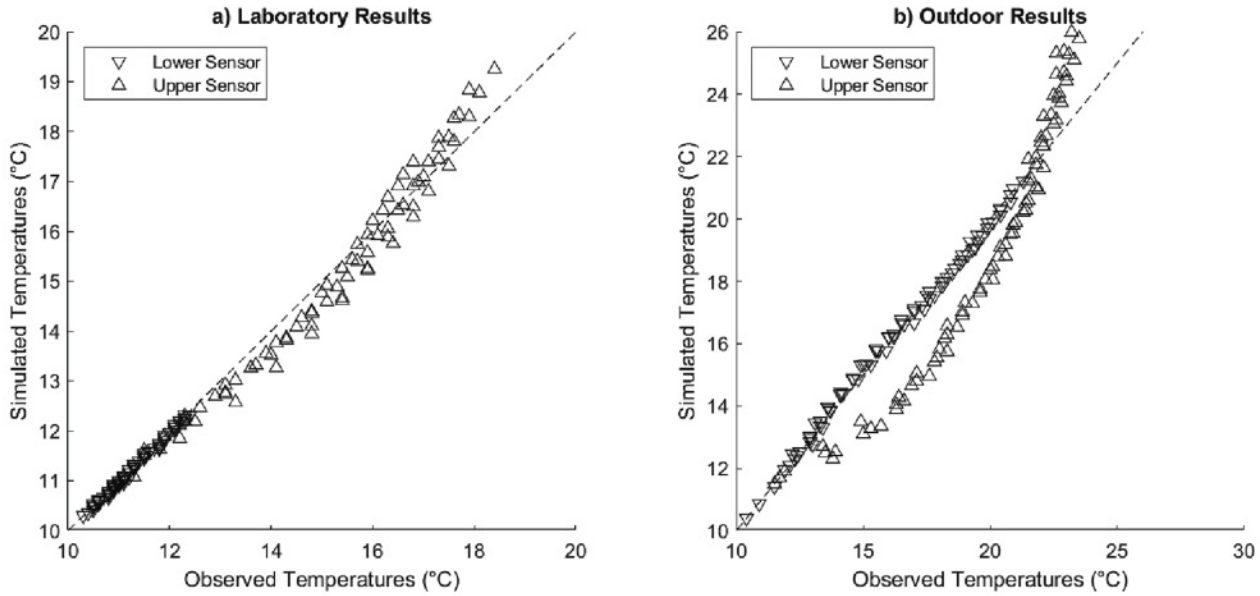

Fig. 5. Scatter plots of observed and simulated temperatures in the (a) laboratory experiments and (b) outdoor experiments.

not directly transferable to Pyramid Lake. As the terminus of an endorheic basin, Pyramid Lake has unique water quality and chemistry; all the dissolved and suspended constituents in the Pyramid water column will contribute to the albedo and attenuation rate of the lake as a whole. Results of the experiments and modeling indicate that DBC could potentially drive increased temperatures in Pyramid Lake, but further work is needed to fully understand and quantify the influence of DBC on the lake's heat balance. For example, similar experiments could be run with water collected from Pyramid Lake itself to determine how DBC changes the transmissive and reflective properties of Pyramid Lake.

3.3. Photoalteration of DBC

Spectral analysis of the DBC before and after the heating experiment showed that little chemical change was imparted during two hours of heat-lamp exposure, but that exposure to the solar spectrum for three hours caused DBC particle size to decrease (E2/E3 shifting from 1.49 to 1.62 to 1.83–1.99), aromaticity to increase (SUVA254 shifting from 13.7 to 14.9 to 17.8–19.8), and CDOM to increase by 8–21 % (Table 3). These shifts are opposite to those seen in photodegradation assessments of biomolecule-derived DBC (Fu et al., 2016), and could represent fullerene oxidation to aromatic fullerene epoxides (Dattani et al., 2015; Tajima et al., 2012). While the C_{60} and C_{70} fullerenes used to generate DBC for the heating experiments are not known to be produced by wildfire combustion of organics (Becker et al., 1995), the behavior of these elemental carbon molecules in the heating trial experiments may give insight to important environmental behavior of other elemental and refractory DBC fractions.

4. Conclusions and potential impacts to surface waters

This work showed that, during peak wildfire activity, DBC was present in Pyramid Lake at levels higher than reported for other large lakes which persisted for 10 months, that DBC was a significant component of the optically active dissolved organic matter in the lake, and that the addition of elemental DBC standards to pure water exposed to the solar spectrum caused an increase in the total amount of radiation entering the water column through a decrease in the surface albedo and subsequently accelerated water heating. These conclusions point to the potential for DBC to contribute to or drive of surface water heating in the environment, particularly in wildfire-impacted regions experiencing increased DBC inputs via deposition. Additional work is required to determine if analogous heating results could be observed in environmental waters with biomass-derived DBC. In lakes, this theorized epilimnion heating could drive increases in mean annual lake temperatures over time, which would have significant ecological implications since temperature is a main driver of aquatic organism distribution and life cycle processes (Magnuson et al., 1979; Dunham et al., 2003). If DBC accumulates over time, compounded heating events could further exacerbate the resulting impacts to ecological functionality. In Pyramid Lake, increases in water temperature above those already predicted as a result of a warming climate (Hostetler and Giorgi, 1995), or an

Table 3
Optimized values for surface albedo and attenuation rates for experimental treatments (Exp) and controls (Ctl) from heating experiments (HE), and spectral parameters of DBC measured at experiment initiation (init) and conclusion (fin).

	HE_40ppb	HE_40ppb_duplicate	HE_30ppb	HE_30ppb_duplicate	HE_90ppb
Surface Albedo, Ctl	0.72	0.75	0.37	0.37	0.37
Surface Albedo, Exp	0.73	0.74	0.35	0.34	0.34
Attenuation Rate, Ctl (m^{-1})	12.2	13.9	7.21	7.21	7.21
Attenuation Rate, Exp (m^{-1})	13.9	14.9	6.99	7.05	6.80
E2/E3, init	1.88	1.58	1.62	1.51	1.49
E2/E3, fin	1.87	1.68	1.99	1.96	1.83
SUVA254, init	20.5	24.0	14.9	13.7	14.7
SUVA254, fin	19.1	23.6	19.8	17.9	17.8
CDOM, init	116	132	70.7	67.9	192
CDOM, fin	108	135	84.0	82.1	208

accelerated rate of heat accumulation caused by high DBC inputs, would cause elevated stress to both the Lahontan Cutthroat trout and Cui-ui fish species in the lake, both of which require cold water temperatures for healthy spawning and recruitment (Scoppettone et al., 1993; Dickerson and Vinyard, 1999). These implications are applicable to all wildfire-impacted surface waters with temperature sensitive species and food webs.

5. Limitations and future research

These results show that the presence of DBC in water affects the surface albedo of the water and the attenuation rates of radiation. The effects of DBC appear to be different for radiation spectra dominated by infrared vs. visible light, with the effects on visible light much more important than those in IR radiation. However, this study did not fully account for wavelength-dependent attenuation or for the wide-ranging and continuous spectrum of solar radiation and did not consider the influence of environmental factors on the surface energy balance of the water column. These experiments show a qualitative impact of DBC on the absorption of light by water but are not sufficient to quantify that impact. Additionally, the elemental DBC used in the heating experiments is not representative of the chemically diverse suite of DBC that results from wildfire combustion of organics. The way that DBC may interact with other DOM fractions found in lake waters is unknown and was not a focus of this study. Finally, a limited number of water samples and replicates were analyzed and the SP2 methodology used to quantify DBC detects only the highly elemental and refractory portion of the DBC.

Additional studies should be conducted in both the near-term and long-term in order to quantify the likely impacts of DBC on Pyramid Lake and similar surface water bodies. Future studies should consider the full solar spectrum and wavelength-specific measurements of albedo and attenuation rate. Additional heating experiments should also be conducted using biomass-derived BC as parent material for DBC preparation and water from Pyramid Lake. More extensive organic analysis methods should be applied to further characterize the DBC within Pyramid Lake, and the effect of DBC on water heating should be compared with heating effects from other organic matter fractions. It is critical that multiple locations and depths within Pyramid Lake and the Truckee River source water are monitored regularly for DBC content over time, to better understand whether DBC accumulates in surface waters and to constrain DBC circulation and removal patterns. The potential association between DBC and other emerging contaminants of concern should be examined, particularly the potential for physical interaction or association between DBC and microplastics which could have additional implications on water heating dynamics. Finally, as more evidence becomes available, careful consideration should be given to the Pyramid Lake food web and how DBC might ultimately impact the ecosystem and PLPT wellbeing.

CRediT authorship contribution statement

Brittany R. Kruger: Conceptualization, Methodology, Investigation, Validation, Data curation, Writing – original draft, Project administration. **Mark B. Hausner:** Methodology, Investigation, Validation, Data curation, Writing – review & editing. **Nathan Chellman:** Investigation, Validation, Data curation, Writing – review & editing. **Morgan Weaver:** Investigation, Resources. **Vera Samburova:** Methodology, Investigation, Validation, Writing – review & editing. **Andrey Khlystov:** Methodology, Writing – review & editing.

Data availability

A submission to DataDryad will include all project data. This will be submitted upon completion of the review process to ensure all reviewer-requested data is included. Also available upon request.

Declaration of competing interest

The authors declare that they have no known competing financial interests or personal relationships that could have appeared to influence the work reported in this paper.

Acknowledgements

The authors extend their sincere gratitude to the Pyramid Lake Paiute Tribe for allowing and supporting this work. Particular thanks are due to the Pyramid Lake Tribal Fisheries Department, especially Mervin Wright (Fisheries Director), Dan Mosley (former Fisheries Director), Jennessy Toribio, Jack Yellowhair, and Michelle Moore. Without their insight, equipment, and sampling assistance this work would not have been possible.

Funding

This work was supported by the Lander Research Fund, administered by the Desert Research Institute.

Appendix A. Supplementary data

Supplementary data to this article can be found online at https://doi.org/10.1016/j.scitotenv.2023.164141.

References

Abatzoglou, J.T., Kolden, C.A., 2011. Climate change in Western US deserts: potential for increased wildfire and invasive annual grasses. Rangel. Ecol. Manag. 64 (5), 471–478. https://doi.org/10.2111/REM-D-09-00151.1.

Ahlberg, E., Ausmeel, S., Nilsson, L., et al., 2023. Measurement report: black carbon properties and concentrations in southern Sweden urban and rural air – the importance of long-range transport. Atmos. Chem. Phys. 23 (5), 3051–3064. https://doi.org/10.5194/acp-23-3051-2023.

Arienzo, M.M., Maezumi, S.Y., Chellman, N.J., Iriarte, J., 2019. Pre-Columbian fire management linked to refractory black carbon emissions in the Amazon. Fire. 2 (2), 31. https://doi.org/10.3390/fire2020031.

Baldock, J.A., Smernik, R.J., 2002. Chemical composition and bioavailability of thermally altered Pinus resinosa (red pine) wood. Org. Geochem. 33 (9), 1093–1109. https://doi.org/10.1016/S0146-6380(02)00062-1.

Becker, L., Bada, J.L., Bunch, T.E., 1995. Fullerenes in the K/T boundary: are they a result of global wildfires? Lunar and Planetary Science Conference. vol 26

Bird, M.I., Moyo, C., Veenendaal, E.M., Lloyd, J., Frost, P., 1999. Stability of elemental carbon in a savanna soil. Glob. Biogeochem. Cycles 13 (4), 923–932.

Bisiaux, M.M., Edwards, R., Heyvaert, A.C., et al., 2011. Stormwater and fire as sources of black carbon nanoparticles to Lake Tahoe. Environ. Sci. Technol. 45 (6), 2065–2071. https://doi.org/10.1021/es103819v.

Burkhard, L.P., Cook, P.M., Lukasewycz, M.T., 2008. Organic carbon – water concentration quotients (Πsocs and πpocs): measuring apparent chemical disequilibria and exploring the impact of black carbon in Lake Michigan. Environ. Sci. Technol. 42 (10), 3615–3621. https://doi.org/10.1021/es702652b.

Byčenkienė, S., Dudoitis, V., Ulevicius, V., 2014. The use of trajectory cluster analysis to evaluate the long-range transport of black carbon aerosol in the South-Eastern Baltic Region. Adv. Meteorol. 2014, e137694. https://doi.org/10.1155/2014/137694.

Caldor Post-Fire BAER Information - InciWeb the Incident Information System. https://inciweb.nwcg.gov/incident/7842/. (Accessed 23 August 2022).

Chellman, N.J., McConnell, J.R., Heyvaert, A., Vannière, B., Arienzo, M.M., Wennrich, V., 2018. Incandescence-based single-particle method for black carbon quantification in lake sediment cores. Limnol. Oceanogr. Methods 16 (11), 711–721. https://doi.org/10.1002/lom3.10276.

Dattani, R., Gibson, K.F., Few, S., et al., 2015. Fullerene oxidation and clustering in solution induced by light. J. Colloid Interface Sci. 446, 24–30. https://doi.org/10.1016/j.jcis.2015.01.005.

De Haan, H., De Boer, T., 1987. Applicability of light absorbance and fluorescence as measures of concentration and molecular size of dissolved organic carbon in humic Lake Tjeukemeer. Water Res. 21 (6), 731–734.

Dickerson, B.R., Vinyard, G.L., 1999. Effects of high chronic temperatures and diel temperature cycles on the survival and growth of Lahontan cutthroat trout. Trans. Am. Fish. Soc. 128 (3), 516–521. https://doi.org/10.1577/1548-8659(1999)128<0516:EOHCTA>2.0.CO;2.

Dixie Fire Incident Report. https://www.fire.ca.gov/incidents/2021/7/13/dixie-fire/. (Accessed 23 August 2022).

Dunham, J., Schroeter, R., Rieman, B., 2003. Influence of maximum water temperature on occurrence of Lahontan cutthroat trout within streams. N. Am. J. Fish Manag. 23 (3), 1042–1049.

Flanner, M.G., Zender, C.S., Randerson, J.T., Rasch, P.J., 2007. Present-day climate forcing and response from black carbon in snow. J. Geophys. Res. Atmos. 112 (D11). https://doi.org/10.1029/2006JD008003.

Flannigan, M.D., Stocks, B.J., Wotton, B.M., 2000. Climate change and forest fires. Sci. Total Environ. 262 (3), 221–229.

Fu, H., Liu, H., Mao, J., et al., 2016. Photochemistry of dissolved black carbon released from biochar: reactive oxygen species generation and phototransformation. Environ. Sci. Technol. 9 Published online.

Galat, D.L., Lider, E.L., Vigg, S., Robertson, S.R., 1981. Limnology of a large, deep, North American terminal lake, Pyramid Lake, Nevada, U.S.A. In: Williams, W.D. (Ed.), Salt Lakes. Developments in Hydrobiology. Springer Netherlands, pp. 281–317 https://doi.org/10.1007/978-94-009-8665-7_22.

Gleason, K.E., McConnell, J.R., Arienzo, M.M., Sexstone, G.A., Rahimi, S., 2022. Black carbon dominated dust in recent radiative forcing on Rocky Mountain snowpacks. Environ. Res. Lett. 17 (5), 054045.

González-Pérez, J.A., González-Vila, F.J., Almendros, G., Knicker, H., 2004. The effect of fire on soil organic matter—a review. Environ. Int. 30 (6), 855–870. https://doi.org/10.1016/j.envint.2004.02.003.

Hamer, U., Marschner, B., Brodowski, S., Amelung, W., 2004. Interactive priming of black carbon and glucose mineralisation. Org. Geochem. 35 (7), 823–830.

Harris, E.E., 1970. Reconnaissance Bathymetry of Pyramid Lake, Washoe County, Nevada. U.S. Geological Survey Hydrologic Investigations Atlas HA-379.

Hausner, M.B., Wilson, K.P., Gaines, D.B., Suárez, F., Tyler, S.W., 2013. The shallow thermal regime of devils hole, Death Valley National Park. Limnol. Oceanogr. Fluids Environ. 3 (1), 119–138.

Helms, J.R., Stubbins, A., Ritchie, J.D., Minor, E.C., Kieber, D.J., Mopper, K., 2008. Absorption spectral slopes and slope ratios as indicators of molecular weight, source, and photobleaching of chromophoric dissolved organic matter. Limnol. Oceanogr. 53 (3), 955–969.

Hostetler, S.W., Giorgi, F., 1995. Effects of a 2$\times$ CO2 climate on two large lake systems: Pyramid Lake, Nevada, and Yellowstone Lake, Wyoming. Glob. Planet. Chang. 10 (1–4), 43–54.

Hudson, J.J., Taylor, W.D., Schindler, D.W., 1999. Planktonic nutrient regeneration and cycling efficiency in temperate lakes. Nature. 400 (6745), 659–661. https://doi.org/10.1038/23240.

Iglesias, V., Balch, J.K., Travis, W.R., 2022. US fires became larger, more frequent, and more widespread in the 2000s. Sci. Adv. 8 (11) eabc0020.

Jacobson, M.Z., 2001. Strong radiative heating due to the mixing state of black carbon in atmospheric aerosols. Nature. 409 (6821), 695–697. https://doi.org/10.1038/35055518.

Jacobson, M.Z., 2002. Control of fossil-fuel particulate black carbon and organic matter, possibly the most effective method of slowing global warming. J. Geophys. Res. Atmos. 107 (D19). https://doi.org/10.1029/2001JD001376 ACH 16-1-ACH 16-22.

Jolly, W.M., Cochrane, M.A., Freeborn, P.H., et al., 2015. Climate-induced variations in global wildfire danger from 1979 to 2013. Nat. Commun. 6 (1), 7537. https://doi.org/10.1038/ncomms8537.

Kaspari, S., McKenzie Skiles, S., Delaney, I., Dixon, D., Painter, T.H., 2015. Accelerated glacier melt on Snow Dome, Mount Olympus, Washington, USA, due to deposition of black carbon and mineral dust from wildfire. J. Geophys. Res. Atmos. 120 (7), 2793–2807. https://doi.org/10.1002/2014JD022676.

Li, M., Bao, F., Zhang, Y., Sheng, H., Chen, C., Zhao, J., 2019. Photochemical aging of soot in the aqueous phase: release of dissolved black carbon and the formation of 1O2. Environ. Sci. Technol. 53 (21), 12311–12319.

Liu, Y., Stanturf, J., Goodrick, S., 2010. Trends in global wildfire potential in a changing climate. For. Ecol. Manag. 259 (4), 685–697. https://doi.org/10.1016/j.foreco.2009.09.002.

Magnuson, J.J., Crowder, L.B., Medvick, P.A., 1979. Temperature as an ecological resource. Am. Zool. 19 (1), 331–343.

Masiello, C.A., Druffel, E.R.M., 1998. Black carbon in deep-sea sediments. Science. 280 (5371), 1911–1913.

Masiello, C.A., Druffel, E.R.M., 2001. Carbon isotope geochemistry of the Santa Clara River. Glob. Biogeochem. Cycles 15 (2), 407–416. https://doi.org/10.1029/2000GB001290.

McConnell, J.R., Chellman, N.J., Mulvaney, R., et al., 2021. Hemispheric black carbon increase after the 13th-century Māori arrival in New Zealand. Nature. 598 (7879), 82–85. https://doi.org/10.1038/s41586-021-03858-9.

Mori, T., Kondo, Y., Ohata, S., et al., 2014. Wet deposition of black carbon at a remote site in the East China Sea. J. Geophys. Res. Atmos. 119 (17), 10485–10498. https://doi.org/10.1002/2014JD022103.

Nash, J.E., Sutcliffe, J.V., 1970. River flow forecasting through conceptual models part I—a discussion of principles. J. Hydrol. 10 (3), 282–290.

Nguyen, B.T., Lehmann, J., 2009. Black carbon decomposition under varying water regimes. Org. Geochem. 40 (8), 846–853.

NPCS Solar Calendars. https://midcdmz.nrel.gov/apps/cal.pl?site=NPC. (Accessed 23 August 2022).

Petzold, A., Ogren, J.A., Fiebig, M., et al., 2013. Recommendations for reporting "black carbon" measurements. Atmos. Chem. Phys. 13 (16), 8365–8379.

Qu, X., Fu, H., Mao, J., Ran, Y., Zhang, D., Zhu, D., 2015. Chemical and Structural Properties of Dissolved Black Carbon Released From Biochars. Published online October 24.

Samburova, V., Connolly, J., Gyawali, M., et al., 2016. Polycyclic aromatic hydrocarbons in biomass-burning emissions and their contribution to light absorption and aerosol toxicity. Sci. Total Environ. 568, 391–401. https://doi.org/10.1016/j.scitotenv.2016.06.026.

Scoppettone, G.G., Buettner, M.E., Rissler, P.H., 1993. Effect of four fluctuating temperature regimes on cui-ui,*Chasmistes cujus*, survival from egg fertilization to swim-up, and size of larvae produced. Environ. Biol. Fish 38 (4), 373–378. https://doi.org/10.1007/BF00007531.

Sengupta, D., Samburova, V., Bhattarai, C., et al., 2018. Light absorption by polar and non-polar aerosol compounds from laboratory biomass combustion. Atmos. Chem. Phys. 18 (15), 10849–10867.

Staley, D.O., Jurica, G.M., 1972. Effective atmospheric emissivity under clear skies. J. Appl. Meteorol. Climatol. 11 (2), 349–356.

Stephens, M., Turner, N., Sandberg, J., 2003. Particle identification by laser-induced incandescence in a solid-state laser cavity. Appl. Opt. 42 (19), 3726–3736.

Stocker, T.F., Qin, D., Plattner, G.K., et al., 2013. Climate Change 2013: The Physical Science Basis. Cambridge University Press Cambridge.

Tajima, Y., Takeshi, K., Shigemitsu, Y., Numata, Y., 2012. Chemistry of fullerene epoxides: synthesis, structure, and nucleophilic substitution-addition reactivity. Molecules. 17 (6), 6395–6414. https://doi.org/10.3390/molecules17066395.

Torres, A., Bond, T.C., Lehmann, C.M.B., Subramanian, R., Hadley, O.L., 2014. Measuring organic carbon and black carbon in rainwater: evaluation of methods. Aerosol Sci. Technol. 48 (3), 239–250. https://doi.org/10.1080/02786826.2013.868596.

Tran, P.Q., Bachand, S.C., McIntyre, P.B., et al., 2021. Depth-discrete metagenomics reveals the roles of microbes in biogeochemical cycling in the tropical freshwater Lake Tanganyika. ISME J. 15 (7), 1971–1986. https://doi.org/10.1038/s41396-021-00898-x.

Van Dorn, W.G., 1956. Large-volume water samplers. EOS Trans. Am. Geophys. Union 37 (6), 682–684.

Wagner, S., Jaffé, R., Stubbins, A., 2018. Dissolved black carbon in aquatic ecosystems. Limnol. Oceanogr. Lett. 3 (3), 168–185. https://doi.org/10.1002/lol2.10076.

Weishaar, J.L., Aiken, G.R., Bergamaschi, B.A., Fram, M.S., Fujii, R., Mopper, K., 2003. Evaluation of specific ultraviolet absorbance as an indicator of the chemical composition and reactivity of dissolved organic carbon. Environ. Sci. Technol. 37 (20), 4702–4708.

Westerling, A.L., Bryant, B.P., 2008. Climate change and wildfire in California. Clim. Chang. 87 (S1), 231–249. https://doi.org/10.1007/s10584-007-9363-z.

Westerling, A.L., Hidalgo, H.G., Cayan, D.R., Swetnam, T.W., 2006. Warming and earlier spring increase western US forest wildfire activity. science. 313 (5789), 940–943.

Wuebbles, D.J., Fahey, D.W., Hibbard, K.A., 2017. Climate Science Special Report: Fourth National Climate Assessment. vol. I Published online.

Xu, F., Wei, C., Zeng, Q., et al., 2017. Aggregation behavior of dissolved black carbon: implications for vertical mass flux and fractionation in aquatic systems. Environ. Sci. Technol. 51 (23), 13723–13732. https://doi.org/10.1021/acs.est.7b04232.

Zigah, P.K., Minor, E.C., Werne, J.P., 2012. Radiocarbon and stable-isotope geochemistry of organic and inorganic carbon in Lake Superior. Glob. Biogeochem. Cycles 26 (1). https://doi.org/10.1029/2011GB004132.